Unified picture of electron and hole relaxation pathways in semiconductor quantum dots

Ryan R. Cooney, Samuel L. Sewall, Eva A. Dias, D. M. Sagar, Kevin E. H. Anderson, and Patanjali Kambhampati*
Department of Chemistry, McGill University, Montreal, Quebec, Canada H3A 2K6
(Received 18 April 2007; revised manuscript received 16 May 2007; published 7 June 2007)

Size dependent electron and hole relaxation dynamics were measured in colloidal CdSe quantum dots with state-to-state specificity. These experiments reveal the electron and hole state-to-state relaxation dynamics with a precision of ~10 fs, allowing quantitative evaluation of the manifold of pathways by which an exciton relaxes in strongly confined quantum dots. These experiments corroborate previously observed confinement induced femtosecond Auger relaxation channels for electrons, but with sufficient precision to quantitatively and unambiguously determine the size dependence of the Auger mechanism. These experiments also show that the hole energy loss rate increases for smaller quantum dots, contradicting known relaxation mechanisms for holes. We propose a confinement enhanced mechanism for hole relaxation in colloidal quantum dots, overcoming the predicted phonon bottleneck for holes. The relative contributions of the relaxation pathways are identified for electrons and for holes. These state selective experiments produce a unified picture of the manifold of relaxation pathways available to both electrons and holes in strongly confined colloidal quantum dots.

DOI: 10.1103/PhysRevB.75.245311 PACS number(s): 78.47.+p, 78.67.Hc, 73.21.La

I. INTRODUCTION

The manner in which an excited exciton relaxes in a semiconductor quantum dot has been under intense experimental[1–21] and theoretical[1,2,20,22–28] investigation for nearly two decades. Despite this effort, a rigorous picture of all relevant processes which determine electron and hole relaxation dynamics in quantum dots remains unresolved. Absorption of a photon creates an exciton for which the electron, hole, or both carriers may be electronically hot.[1,2,12] Quantum confinement of the charge carriers results in atomiclike envelope states for the electrons and the holes.[20,29–32] Since confinement results in a resolvable eigenstate spectrum for semiconductor quantum dots, the electronic level spacings will be larger than for bulk semiconductors. This increase in energy level spacing was expected to have a dramatic effect on the rates of dissipation of excess electronic energy of the exciton.[1,2,20]

An understanding of the rates and pathways by which excitons relax in quantum dots is important both for understanding the fundamental physics of relaxation pathways in nanoscale solids,[1,2,20] as well as for utilizing quantum dots in applications.[33] Quantum dots may be used in light emitting diodes, photovoltaic cells, and lasers. For example, interband visible lasers would benefit from fast electronic relaxation to the band edge, whereas intraband midinfrared lasers would require slow dynamics. Solar energy conversion using quantum dots may be made more efficient by slowing down carrier cooling.[2,33,34] The new physics of multiple exciton generation makes this question still more compelling.[33,34] Recent theoretical work by Shabaev *et al.* on multiple exciton generation suggests that one of the key problems is that a precise understanding of exciton relaxation dynamics remains unresolved.[35] Rational design of quantum dot materials must begin with a rigorous understanding of how spatial and electronic structures determine electronic relaxation pathways.

This paper reports on the size dependent relaxation pathways of electrons and holes in colloidal CdSe quantum dots with state-to-state specificity. Since the initial and the final excitonic states are spectroscopically prescribed while maintaining femtosecond time resolution, we were able to quantitatively measure the excitonic state-to-state transition rate as a function of particle size. By holding the states constant for each size of quantum dot, significant improvement was made in the ability to evaluate the size dependent relaxation pathways of excitons in quantum dots. We find that electrons relax primarily via Auger processes with a precise size dependence, which results in faster transition rates for smaller particles. In contrast, holes relax primarily by a surface ligand mediated nonadiabatic process, which results in a size independent transition rate. The broad result is that electrons and holes relax via *several* competing quantum dynamical pathways. The *relative* contributions from each relaxation pathway were determined by precision measurements of the state-to-state transition rates.

II. BACKGROUND

Much experimental[1–19,21,36] and theoretical[1,2,22–28] work has been done on evaluating the relaxation dynamics of hot excitons in semiconductor quantum dots. Due to the larger electronic level spacings from quantum confinement,[29–31] early theory predicted that *electron* relaxation should be slower for quantum confined structures.[1,2,22,23,27] This phonon "bottleneck" was expected as multiphonon emission via the Fröhlich interaction would be required to climb down the manifold of electronic states. The electronic energy gaps are ~150–350 meV,[30–32] in comparison to the longitudinal optical (LO) phonon energy of ~30 meV.

In contrast to these predictions, experimental measurements showed fast subpicosecond electron relaxation dynamics in colloidal semiconductor quantum dots.[1,3,6,7] More recent theory proposed the presence of a confinement enhanced Auger relaxation pathway in which the electron unidirectionally transfers energy to the hole.[24–26] This process can be fast in quantum dots due to larger wave function overlap and reduction in momentum conservation requirements due to spatial localization. Experiments have qualita-

tively shown that smaller particles have faster electronic relaxation rates, consistent with the presence of an ultrafast Auger channel for electrons. Theory has predicted that the electron relaxation times are ~0.1–2 ps, with a size dependence in which rate could be flat or decreasing with particle radius.[24,26]

An alternative situation was probed in which the hole was spatially decoupled from the electron.[4,5,8,21] The femtosecond Auger channel requires the presence of the hole in order to accept the excess energy from the electron. In the event that the hole is decoupled from the electron, the Auger channel becomes deactivated for the electron. Thus, a spatially decoupled hole would allow for observation of the electron dynamics in isolation from the hole. Decoupling of the hole was achieved by using hole traps at the surface of the colloidal quantum dot[4,5,8] or by nongeminate carrier capture in epitaxially grown quantum dots.[21] In the case of the epitaxially grown quantum dots, ligands are absent and a phonon bottleneck was observed.[21] In a sequential pumping scheme, experiments by Guyot-Sionnest *et al.* and Klimov *et al.* on colloidal quantum dots showed that the electron dynamics proceeds on the 3–30 ps time scale in the absence of the femtosecond Auger channel. The experiments by Guyot-Sionnest *et al.*[4,5] furthermore showed that under these circumstances, the surface ligands had a pronounced effect on the time scale of electron relaxation from $1P$ to $1S$. These experiments showed that in the absence of the Auger channel, the electron relaxes on a picosecond time scale. These experiments furthermore showed that the pathway for electron relaxation has a dominant contribution from a surface ligand based channel, provided that the Auger channel is removed.

While the electron has a femtosecond Auger channel in CdSe quantum dots, the holes do not. The electron level spacings are approximately three times greater than the hole level spacings for CdSe quantum dots. As such, it was expected that the holes should have a phonon bottleneck at the final stages of relaxation near the band edge.[5,10,20] Experiments by Xu *et al.*[10] and subsequently by Hendry *et al.*[19] probed relaxation dynamics of the hole. Xu *et al.* used a combination of transient absorption (TA) and transient photoluminescence (PL) to monitor hole relaxation.[10] These experiments suggest that the hole relaxation slows down closer to the valence band edge due to the sparser density of states at the band edge. These experiments furthermore suggest that there was a phonon bottleneck near the band edge for the holes. However, these experiments were not able to monitor state-to-state dynamics and furthermore cannot measure the relevant dynamics with the 10 fs precision required for quantitative determination of the state-to-state transition rate for holes.

A key difficulty in spectroscopic experiments on quantum dots is that both initial and final excitonic states need to be spectroscopically prescribed. For example, with fixed excitation wavelengths, larger particles will necessarily measure electron and hole relaxation dynamics. In all but the smallest particles, the hole will get up pumped by the electron and then relax through the valence band. Regardless of the instrumental time resolution, photoluminescence measurements cannot measure the hole dynamics of interest with *quantitative* precision. Specificity in the *final* hole state was achieved by Hendry *et al.* using time resolved terahertz spectroscopy.[19] These experiments monitored the arrival time of the hole to the band edge from an arbitrary initial state. The initial state depended upon the size of the quantum dot. These experiments suggested that the arrival time of the hole was ~350 fs, provided that the electron was initially in its lowest energy $1S$ state. The key point is that no prior experiment has been able to monitor the hole dynamics with *specificity* in the initial and the final excitonic states, along with the time resolution needed to *quantitatively* measure the relevant processes.

While exciton relaxation dynamics in semiconductor quantum dots has been extensively studied, a clear and quantitative picture of the relevant processes is lacking. The key difficulty is due to the size dependent eigenstate spectrum.[12,29–32] This size dependence means that the same initial excitonic states are not necessarily populated for each size of quantum dot.[12] Furthermore, since these are multilevel systems, the relaxation dynamics will not necessarily be characterized by simple functions which represent transition rates.[12] For example, many experiments use the pump-probe (transient absorption) scheme. These experiments commonly use excitation at 400 nm (3.1 eV). Under these excitation conditions, the electron will not necessarily be initially prepared in its $1P$ state. Instead, the electron will be in the $2S$ or higher lying state.[12] Thus, the electron relaxation will follow sequential kinetics. An additional difficulty is that the density of states shows that the initial electronic state could be a mixture of $1S$, $1P$, or $2S$. Thus, the measured electron relaxation will follow a sum of three signals consisting of a step function, single exponential, and nonexponential, convolved with the instrument response function (IRF),

$$\Delta\mathrm{OD}(t) = \left\{ A_{1S} + A_{1P}e^{-k_1 t} + A_{2S}\left[1 + \frac{1}{k_2 - k_1}(k_1 e^{-k_2 t} - k_2 e^{-k_1 t}) \right] \right\} \otimes \mathrm{IRF}. \tag{1}$$

Here, $k_2 \equiv k_{2S\rightarrow 1P}$ and $k_1 \equiv k_{1P\rightarrow 1S}$. Each k represents the total rate for a state-to-state transition, which is comprised of several pathways which contain the desired dynamical information. Larger particles would follow even more complex kinetics with more highly excited initial states. *Regardless* of pulse duration, it would be impossible to precisely extract a transition rate $k_{1P\rightarrow 1S}$, from a smoothly varying experimental transient. In contrast, an *exciton selective* approach[12,36] can yield *state-to-state* exciton dynamics with specificity to either electron dynamics or hole dynamics,

$$\Delta\Delta\mathrm{OD}(t) = e^{-kt} \otimes \mathrm{IRF}. \tag{2}$$

Here, the k represents a specific state-to-state transition rate, whether for electrons or holes. By using various permutations of pump and probe wavelengths selected to be resonant with specific initial and final states, an exciton selective approach yields electron and hole relaxation dynamics with state-to-state-specificity and a temporal precision of 10 fs,

recovering the pulse width limited precision that one expects for simple two-level systems.[12,36] This temporal precision is essential to quantitatively establish the relative contributions of *multiple* relaxation pathways, each of which may have a distinct size dependence.[12,36]

III. EXPERIMENT

Samples of colloidal CdSe quantum dots were prepared using published procedures.[37] The samples had no apparent deep trap emission and had absorption and emission linewidths characteristic of an ensemble dispersity of $\sigma = 5\% - 10\%$. The sizes of the quantum dots were obtained from published sizing curves.[38] Toluene, methanol, hexanes, and acetone were obtained from Fisher and used as received. All other chemicals were purchased from Aldrich and used as received. The steady state absorption measurements were performed on a Varian Cary 300 UV-visible spectrophotometer. The PL and photoluminescence excitation spectra were measured on a Spex Fluromax-2 spectrofluorometer. For these measurements, the nanocrystals were dissolved in toluene.

The spectroscopic measurements were made using a regeneratively amplified Ti:sapphire laser system (800 nm, 50–60 fs, 1 kHz, and 2.5 mJ; Coherent) in the pump-probe configuration. The probe pulse was derived from single filament white light continuum generated in a 2 mm sapphire crystal. The pump pulses were derived by frequency doubling the 800 nm fundamental beam in a 100 μm β-BaB_2O_4 crystal (BBO), or via optical parametric amplifiers (OPA). The pump wavelengths were tuned to specific initial excitonic states, Fig. 1. Pumping at 400 nm (3.1 eV) was previously done[12] for comparison to prior works.[1,6,7,10,39]

The continuum probe and OPA pump pulses were dispersion compensated by fused silica prism pairs. The IRF was improved from previous measurements[12] to 60–70 fs full width at half maximum (FWHM), over all wavelength combinations. The OPA derived pump pulses were 40–50 fs FWHM in duration and were nearly transform limited, with a time-bandwidth product $\Delta\tau\Delta\nu = 0.45 - 0.50$. The pulse durations and instrument response functions were measured by autocorrelation and cross correlation in 30 μm BBO crystals at the sample position. Autocorrelations were measured to ±100 ps to verify the absence of satellite pulses which can happen due to etaloning inside the regenerative amplifier.

To facilitate precise comparisons of transients at different pump wavelengths, two experiments were performed *simultaneously* by alternately chopping each of the OPA pump beams such that there was shot to shot alternation of the pump color. Two transients were collected at 333 Hz, corresponding to pump-probe experiments at two different pump wavelengths. The frequencies and phases of the two choppers were set to produce a sequence of pump 1, no pump, pump 2. Gated integration was performed on each shot, which was then digitized at 18 bits. Probe ratiometry was performed after spectral selection in order to minimize effects of continuum noise. Pump normalization was performed for each laser shot to further minimize instrument drift and noise. Spot sizes were 300 μm (pump) and 50 μm (probe). Crossing angles were 5° for both pump beams. The time delay between pulses was set by a computer controlled delay stage with 0.1 μm precision.

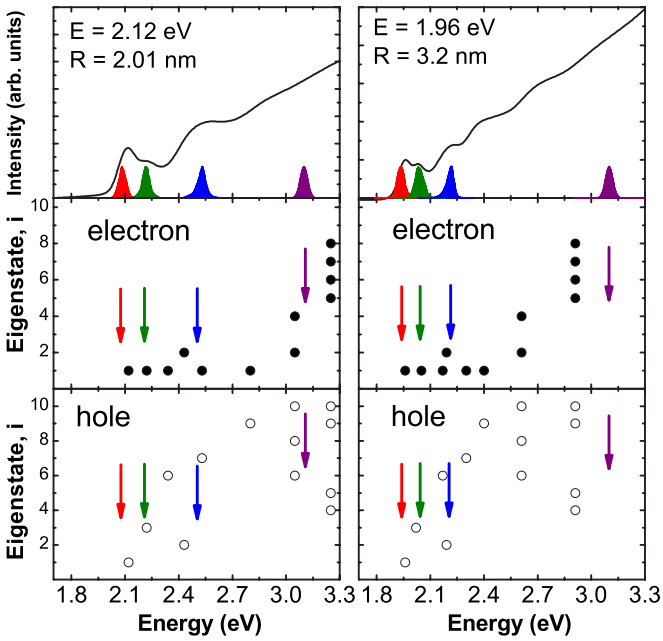

FIG. 1. (Color online) Absorption spectra and laser spectra for two sizes of CdSe quantum dots. The three lowest energy laser spectra are used for the pump pulses in the exciton selective experiments, and the 3.1 eV spectra are common to other experiments which probe relaxation dynamics. The extent of excitation of the electron and hole is shown as a function of photon energy. The extent of excitation is denoted by the ordering of the eigenvalues for the electron and hole. Past 3.0 eV, the transitions overlap, forming a dense quasicontinuum of states.

The sample consisted of quantum dots dispersed in toluene and continuously circulated through a 1 mm path length quartz flow cell at 295 K. The pump fluence was set to maintain the same mean exciton occupancy $\langle N \rangle = 0.5$.[1,39] The OD of the sample was 0.1 to maximize uniformity of the pump intensity throughout the probed volume. Bleach magnitudes were ~50 mOD at the band edge ($B1$) and noise levels were typically ~0.2 mOD. The $A1$ feature was ~5 mOD. The $\Delta\Delta$OD signals were ~20 and 10 mOD for the $B1$ and $A1$ features, respectively. The transient spectral features such as $A1$, $B1$, $B2$, $A2$ were taken from the notation of Klimov *et al.*[1,7]

Step sizes were 10 fs for the first 2 ps. It was verified that there was no power dependence to the transients. Time constants were obtained by fitting the entire transient data to a model function consisting of a sum of exponentials convolved with the IRF. The reproducibility of the methods and results was verified by collecting ten transients per day, for three separate days of experiments, on each of three different syntheses for one size of quantum dot. Uncertainties in the fits were obtained by fitting at least 15–20 transients for each of the different sized samples, resulting in typical standard deviations of ±10 fs.

IV. RESULTS

A. Exciton selectivity and state-to-state dynamics

We have recently shown that an exciton selective pump-probe approach can probe state-to-state exciton transition rates.[12] By pumping into specific initial excitonic states and probing all transient signals, the meaningful combinations of pump-probe wavelengths was obtained. For example, it was found that the band edge bleaching signals only monitor electron relaxation dynamics, despite the presence of a relaxing hot hole. This result allows for monitoring electron dynamics *independent* of hole dynamics. On the other hand, hole dynamics can be obtained by pumping into two initial states which both have a *cold* electron. From a 4×4 matrix of 16 pump-probe configurations, it was found that one pair of configurations yielded state-to-state electron dynamics from $1P_e \rightarrow 1S_e$, and a different pair yielded state-to-state hole dynamics from $2S_{3/2} \rightarrow 1S_{3/2}$.[12] *Most* pump-probe configurations were not useful to precisely and unambiguously extract electron or hole relaxation dynamics.

The key step in a state-to-state approach is spectroscopic selectivity in the initial excitonic state. Due to an overlapping eigenstate spectrum, it is not possible to prepare the electron only in its $1P$ state.[12,29–32] Instead, the electron will be prepared in an admixture of $1S$ and $1P$ states. Subtractive methods, however, can yield the electron dynamics of the $1P$ state.[12] State-to-state hole dynamics can be obtained near the band edge by noting that the electron remains in the cold $1S$ state for the first two excitonic states. The difference between the transients for these two initial excitonic states reflects the hole dynamics only. Thus, exciton selectivity can yield the final stage of hole relaxation with state-to-state specificity.[12,36]

Unraveling state-to-state exciton dynamics using an exciton selectivity employs a time and frequency domain approach. Since some of the dynamics may proceed on the 100 fs time scale, pulses shorter than 100 fs are required to maintain sufficient time resolution to observe all the relevant processes. However, pulses shorter than 30 fs will have too much bandwidth to selectively excite specific initial states. The ideal pulses to maintain the appropriate time *and* frequency resolution should be 30–60 fs in duration, with a bandwidth of 60–30 meV.

The implementation of exciton selectivity is illustrated for two sizes of CdSe quantum dots in Fig. 1. The first three laser spectra were chosen to yield either electron or hole dynamics. The laser spectra at 3.1 eV were previously used[12] for comparison to prior works.[1,6,7,10,39] Excitation at 3.1 eV was used as a reference for one size of quantum dot[12] but was not used here for size dependent relaxation pathway experiments due to its inability to cleanly extract the relevant dynamical processes. The lower panels of Fig. 1 show the ordering of the electron and hole eigenstates[12,31,32] as a function of photon energy. One can see that higher photon energy does not necessarily correspond to a hot electron. Furthermore, the states tend to overlap at higher energy as indicated by vertically offset points at the same energy. Finally, excitation at 3.1 eV results in different initial states based on the size of the quantum dot.

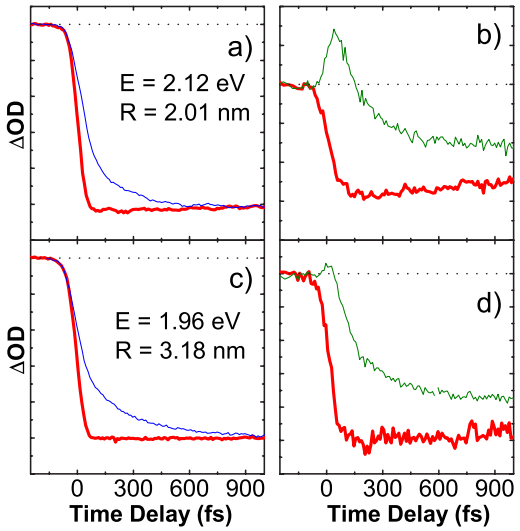

FIG. 2. (Color online) Pump-probe transients which probe either electrons or holes. The left column shows transients at spectral feature $B1$. The thick red line corresponds to lowest energy (red) spectrum in Fig. 1, while the thin blue line corresponds to the second highest energy (blue) spectrum. The right column shows transients at spectral feature $A1$. The thick red line corresponds to lowest energy (red) spectrum in Fig. 1, while the thin green line corresponds to the second lowest energy (green) spectrum. The $B1$ feature only monitors electron dynamics and the $A1$ feature only monitors hole dynamics, for these initial excitonic states. The notation of the transient spectral features is taken from Ref. 1. The dashed line corresponds to the zero level.

Exciton selective pump-probe data for two sizes of colloidal CdSe quantum dots are shown in Fig. 2. Following prior work,[12] the band edge bleaching signal $B1$ was used to extract electron dynamics, Figs. 2(a)–2(c). Pumping into the band edge state ($1S_e$-$1S_{3/2}$) produces an instrument response function (IRF) limited bleach with no dynamics on the subpicosecond time scale. These transients correspond to the red laser spectrum in Fig. 1. The blue laser spectrum in Fig. 1 prepares excitons initially in an admixture of the $1P_e$-$1P_{3/2}$ and the $1S_e$-$2S_{1/2}$ states. Similarly, the subresonant biexciton signal[12,36] $A1$ was used to extract the hole dynamics, Figs. 2(b) and 2(d). These transients correspond to the red ($1S_e$-$1S_{3/2}$) and the green ($1S_e$-$2S_{3/2}$) laser spectra in Fig. 1.

B. Electron and hole survival probabilities

None of these transients directly monitor either electron or hole populations. In the case of electrons, it is not possible to excite excitons for which all quantum dots have the electron initially in the $1P$ state. It is the difference between the two initial excitonic states which yields the $1P$ electron dynamics.[12] Since there are discrete eigenstates, one should rigorously speak of a state-to-state transition rate which reflects the quantum dynamics of the survival probability. Figure 3 shows the $\Delta\Delta$OD transient, which is the difference between the standard pump-probe ΔOD transients.[12] This subtractive procedure was previously implemented by Kambhampati *et al.* on early time dynamics in molecular

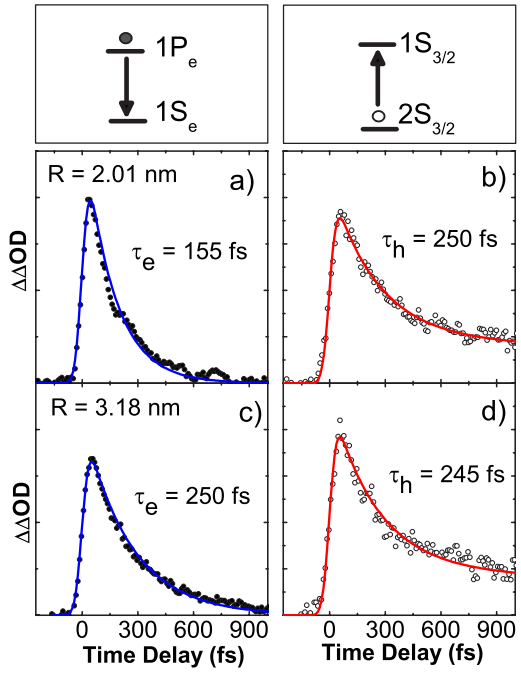

FIG. 3. (Color online) Excited state survival probabilities of electrons and holes. The survival probabilities are monitored by the ΔΔOD transient which is a subtraction of each of the ΔOD transients in Fig. 2. The ΔOD transients are spectroscopically selected to only reflect either electron or hole dynamics. The electron dynamics corresponds to transitions from the $1P_e \rightarrow 1S_e$ electron states. The hole dynamics corresponds to transitions from the $2S_{3/2} \rightarrow 1S_{3/2}$ hole states. The points are the data and the lines are the fits.

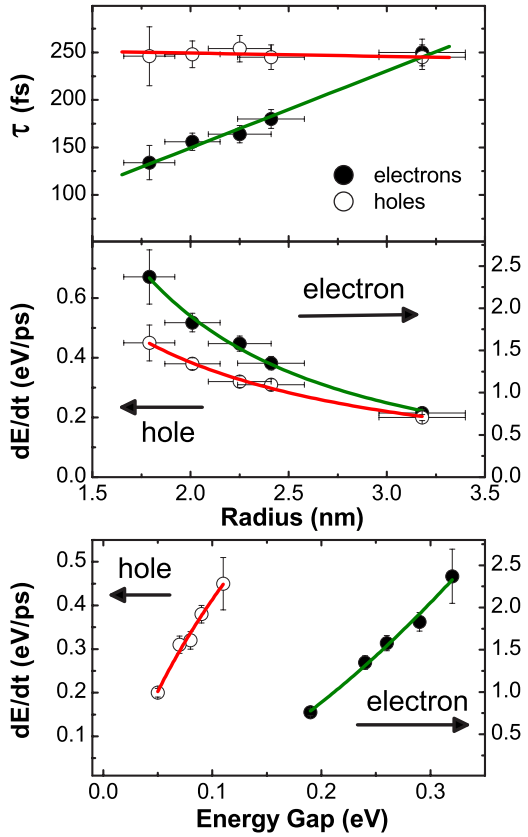

FIG. 4. (Color online) Experimental data for electron and hole relaxation dynamics as a function of particle size. The lines are empirical fits. (a) The lifetimes for the specific state-to-state transitions $1P \rightarrow 1S$ (electron) and $2S_{3/2} \rightarrow 1S_{3/2}$ (hole). (b) The electron and hole energy loss rates as a function of particle radius. Neither electrons nor holes have a phonon bottleneck in strongly confined colloidal quantum dots. (c) The energy loss rates as a function of energy gap corresponding to the above initial and final states.

systems.[40] The ΔΔOD transients monitor the survival probabilities of the hot electrons or holes and therefore reflect the state-to-state transition rate. The $1P$ electron has lifetimes of 155±10 fs for R=2.01 nm and 250±10 fs for R=3.18 nm. These lifetimes correspond specifically to the process $1P_e \rightarrow 1S_e$.

The hole dynamics are also shown in Fig. 3. The green laser spectrum in Fig. 1 reflects excitation into a hot hole state, $1S_e$-$2S_{3/2}$. Since the band edge bleach ($B1$) does not monitor hole dynamics, another spectral feature is needed to probe holes. It was previously shown that the subresonant $A1$ feature is sensitive to the initial excitonic state.[12] This spectral feature probes the bound state of the biexciton.[1,3,7,12,36,41] Pumping into the $1S_e$-$1S_{3/2}$ state produces an IRF limited bleach which decays in a picosecond time scale, whereas pumping into the $1S_e$-$2S_{3/2}$ produces an IRF limited induced absorption which decays on a subpicosecond time scale. For both transients, the electron is initially in the $1S$ state. Hence, the difference between these transients reflects the hole dynamics. The $2S_{3/2}$ hole has lifetimes of 250±10 fs for R =2.01 nm and 245±10 fs for R=3.18 nm. These lifetimes correspond to the process $2S_{3/2} \rightarrow 1S_{3/2}$.

The electron and hole survival probabilities are experimentally monitored by the ΔΔOD transients. In the case of the electron, the survival probability is well fitted by a single exponential. The hole has a majority component on the femtosecond time scale and a minority component on the picosecond time scale. This biexponential behavior was previously observed by Klimov *et al.*[8] and also by Guyot-Sionnest *et al.* for electrons.[4] In that case, a sequential pumping scheme was used to re-excite electrons from $1S$ to $1P$. Biexponential transients were observed, which were assigned to a portion of the excited electrons being trapped at an interface state. Our experiments on holes produce similar results. We assign the picosecond component (10%–20% relative amplitude) to the trapping of the holes at interface states which are not being probed here. Thus, excited state trapping will remove some of the population which manifests itself as either an offset or a slow component to the transient. This point will be further discussed elsewhere.[42] These excited state trapping processes are not unique to semiconductor quantum dots; the same manifestation of excited state removal was also observed in the quantum dynamics of the excited states of an excess electron in solution.[43–45]

The full size dependent experimental data are shown in Fig. 4. The hole data show a lifetime that is independent of particle size within the experimental uncertainty of 10 fs. The size dependent electron lifetime is qualitatively consistent with prior work of Klimov *et al.*[1,6,7] In this prior work, the initial excitonic state was not spectroscopically held con-

stant. This situation resulted in a difficulty in establishing state-to-state transition rates with better than 100 fs precision. The deviations will become more pronounced for the larger quantum dots, for which the electron is in higher lying initial states, in addition to an increased density of states (Fig. 1).[12] Hence, the deviations between these data and the prior data for large quantum dots are not surprising. The key observation for electrons is that the lifetime of the $1P$ state is clearly *linear* to particle radius within the 10 fs precision of these measurements.

The carrier cooling rate (eV/ps) is commonly discussed in prior works to bear correspondence to bulk measurements.[1,2,5–7] Figures 4(b) and 4(c) also show the carrier cooling rate based on the known energy gaps for electrons and holes.[31,32] In the case of electrons and holes, there is clearly an absence of a phonon bottleneck. This result is well established *qualitatively* for electrons and is quantitatively determined here. This result was unexpected for holes and represents another observation.[36] When the cooling rate is plotted as a function of energy gap, it clearly shows the absence of the phonon bottleneck for *both* carriers. While a carrier cooling rate is commonly used in systems with a continuous density of states, a state-to-state transition rate is more appropriate for quantized systems characterized by a resolvable eigenstate spectrum.

V. DISCUSSION

A. Hole relaxation dynamics

1. State-to-state dynamics near the band edge

In quantum confined semiconductors, theory[24–26] and experiment[1–3,6,7] have shown that there is a confinement induced femtosecond relaxation channel for electrons. In this femtosecond channel, the electron *unidirectionally* transfers its energy to the hole through a Coulomb mediated Auger process. This process has an enhanced rate by virtue of greater wave function overlap and a greater momentum space spread by confinement in position space. Yet, the *holes* should have no such channel in CdSe since their energy levels are approximately three times smaller than for electrons.[30–32] Thus, a phonon bottleneck was anticipated for hole dynamics.

Size dependent hole dynamics was previously monitored by using either transient absorption (TA) combined with transient photoluminescence (PL),[10] or by time resolved terahertz experiments.[19] In the first case,[10] the data suggested the presence of a phonon bottleneck for the final stages of hole relaxation where the level spacing becomes large. These TA and PL experiments were not able to specify initial states and did not necessarily have better than 100 fs time resolution. In the second case (terahertz),[19] there was also no specificity in the initial state. The time to reach the band edge state was ~350 fs, qualitatively consistent with these state-to-state measurements. The terahertz measurements, however, had an IRF of ~600 fs as compared to the ~60 fs IRF here. These experiments have the time resolution and the state selectivity to quantitatively measure the state-to-state transition rates for holes. In addition, these state-to-state experiments show that hole dynamics near the band edge is qualitatively different than expected from prior work.

These experiments reveal a size dependent hole relaxation dynamics which clearly shows the presence of a *mechanism which dominates hole relaxation* in colloidal semiconductor quantum dots. We propose a mechanism for the observed size independent state-to-state hole transition rates which involves nonadiabatic interactions. The total rate for hole relaxation will be the sum of individual relaxation channels. The phonon based mechanism is via emission of LO phonons by the Fröhlich interaction.[1,2,22,23,27] The existence of additional channels can be evaluated by quantitatively monitoring the size dependent transition rates. A nonadiabatic relaxation channel was recently assigned for electron relaxation in PbSe quantum dots where the proposed coupling is via the crystallite LO phonons.[11] We propose nonadiabatic coupling to surface ligands based on the size and energy gap dependences of the rate. A nonadiabatic mechanism mediated by surface ligands can quantitatively reproduce the observed size independent transition rates for holes.

Nonadiabatic processes are well known in quantum molecular dynamics[46–59] and have recently been proposed as an electron relaxation channel in PbSe colloidal quantum dots.[11] The state-to-state nonadiabatic transition rate evaluated in a golden rule form [Eq. (1)] will reflect the size dependence of the transition matrix element coupling the initial and final states,

$$k_{fi}(R) = \frac{2\pi}{\hbar}|M_{fi}(R)|^2 \rho(E_f). \tag{3}$$

The transition rate was initially established for LO phonon based relaxation through the Fröhlich interaction and subsequently for Auger relaxation for electrons. The matrix element for nonadiabatic transitions is[49]

$$M_{fi} = \sum_n \frac{-\hbar^2}{\mu_n} \langle \chi_f | \langle \psi_f | \frac{\partial}{\partial Q_n} | \psi_i \rangle \frac{\partial}{\partial Q_n} | \chi_i \rangle. \tag{4}$$

This matrix element describes the coupling of the adiabatic Born-Oppenheimer states. The ψ's represent the adiabatic electronic states, the χ's represent the vibrational states, and Q represents a nuclear coordinate. This electronic portion of the nonadiabatic matrix element can be more explicitly recast by using the Hellman-Feynman theorem as[49]

$$\langle \psi_f | \frac{\partial}{\partial Q} | \psi_i \rangle = \langle \psi_f | \frac{\partial \hat{H}_i}{\partial Q} | \psi_i \rangle / (E_f - E_i). \tag{5}$$

The energy denominator reflects the hole level spacing, which is $E(2S_{3/2}) - E(1S_{3/2})$ for this state-to-state experiment. Assuming harmonic potentials, the Hellman-Feynman force will be proportional to the displacement of the adiabatic potential (ΔQ) for the excited state along the relevant normal coordinate(s),

$$\frac{\partial \hat{H}}{\partial Q} \sim \Delta Q. \tag{6}$$

Assignment of the relaxation mechanism can be obtained by considering the size dependence of the nonadiabatic transition matrix element.

The matrix element depends upon the energy gap and the Hellman-Feynman force. The size dependence of the energy spacing of hole levels will *decrease* the rate for smaller particles as the energy gap gets larger. This contradicts the experimental observation, Fig. 4. The size dependence of the exciton-phonon coupling Δ (or Huang-Rhys parameter S) is known from resonance Raman,[60,61] photon echo,[62,63] and pump-probe experiments. Prior works show that exciton-phonon coupling via LO phonons decreases for smaller particles for CdS,[60] CdSe,[62] InP[64] and PbS.[61,63] Since the force is proportional to ΔQ,[49,65,66] larger particles will have a larger Hellman-Feynman force. This is also opposite to experimental observations. Independent experimental data show that nonadiabatic transitions mediated by LO phonons cannot qualitatively reproduce the observed size dependent state-to-state hole transition rate.

Since nonadiabatic transitions can be induced by any coupled vibrational mode, one must also consider the surface ligands. The influence of surface ligands on electron relaxation dynamics (decoupled hole) was demonstrated by Guyot-Sionnest *et al.*[5] The role of ligands on hole dynamics was modeled by setting ΔQ proportional to the overlap of the hole with the surface ligands.

The wave function of the hole was modeled as a particle in a finite spherical potential, following prior works.[67–70] Within the effective mass and envelope approximations, the wave function can be written as a product of the radial function and spherical harmonics.

$$\Psi(r,\theta,\phi) = R(r)Y_l^m(\theta,\phi). \tag{7}$$

The radial function is written in terms of Bessel and Neumann functions inside the barrier, which reduces to an exponential function outside the barrier,

$$R(r) = Aj_l(kr) + Bn_l(kr), \tag{8}$$

with $k=[2m^*(E-V)/\hbar^2]^{1/2}$. The fractional charge which interacts with the ligands is computed by integrating the wave function from $r=(R-c)\rightarrow\infty$, where R is the radius of the quantum dot and c is the size of an isotropically approximated unit cell of dimension 0.4 nm, and m^* is the effective mass. The fraction of the hole which is in direct contact with the ligand shows a size dependence which is nearly equal to that of the hole energy gap, Fig. 5.

The hole dynamics are modeled by assuming two relaxation channels: LO phonon emission and ligand induced nonadiabatic transitions.[36] Prior works[2,71,72] modeled the phonon based hot carrier lifetime as

$$\tau = \omega_{LO}^{-1}\exp(\Delta E/k_B T). \tag{9}$$

The magnitude of the nonadiabatic channel was adjusted such that the two rates equal the measured rate for one size of the quantum dot. The key result is that the nonadiabatic channel has a size dependent functional form which matches experiment for all sizes. These size dependent channels produce an experimentally determined *total* transition rate, which is nearly size independent, Fig. 6. The nonadiabatic surface channel, in conjunction with minor contribution from the phonon emission channel, quantitatively reproduces the observed size independent state-to-state transition rate for holes.

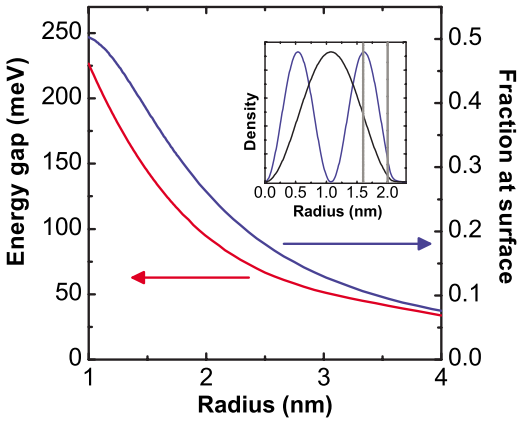

FIG. 5. (Color online) The size dependence of the fraction of the hole envelop function at the surface and of the hole energy gap. The fraction at the surface represents the amount of charge density extending from the outermost unit cells relative to the total volume, including tunneling outside the crystal. The energy gap corresponds to the gap between the final two hole states, $2S_{3/2}$-$1S_{3/2}$, taken from Ref. 29. The inset shows the $1S$ and $2S$ wave functions with a radius of 2.0 nm. The vertical lines represent the last cell.

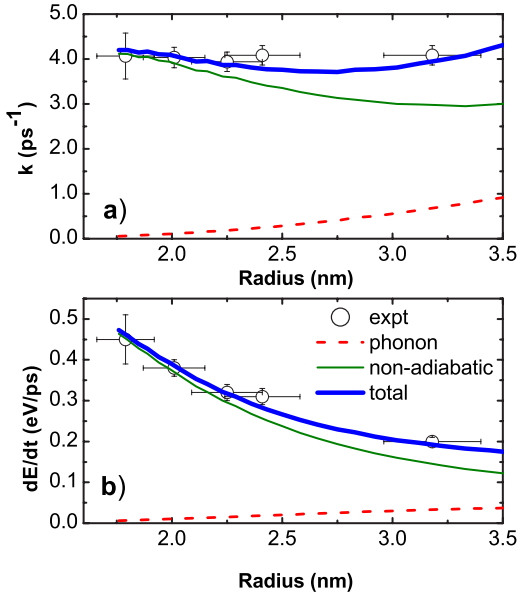

FIG. 6. (Color online) (a) The hole transition rate as a function of particle radius. (b) The hole energy loss rate (dE/dt) as a function of particle radius. The experiment corresponds to hole transitions from $2S_{3/2}\rightarrow 1S_{3/2}$, while the electron remains in the $1S$ state. The phonon channel is for emission of LO phonons, while the surface channel is for nonadiabatic transitions induced by surface ligands.

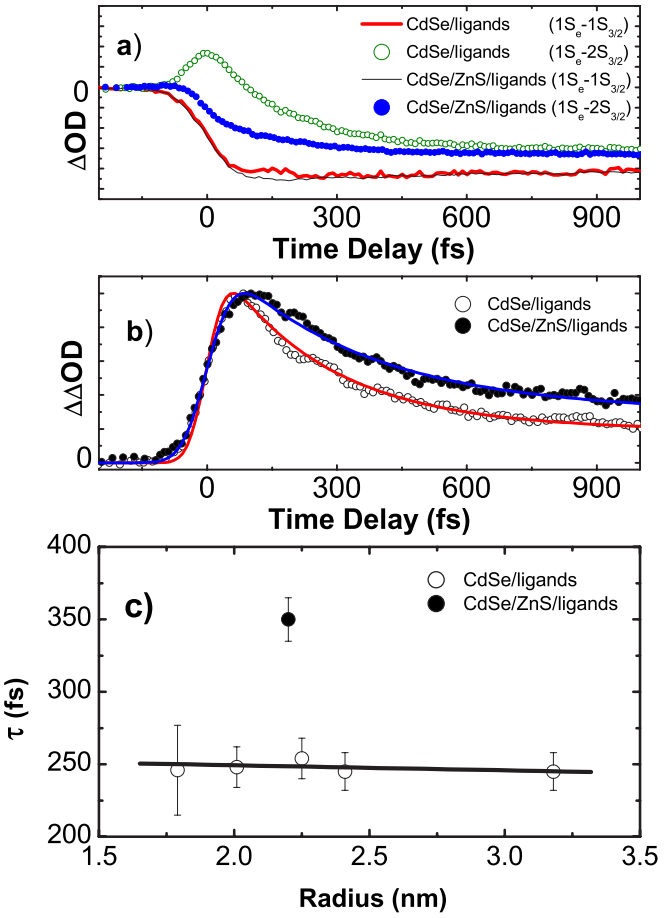

FIG. 7. (Color online) Effect of decoupling the surface ligands upon hole dynamics. (a) The pump-probe transients showing the effect of the ZnS tunneling barrier. The initial excitonic state is noted in parentheses. (b) The hole survival probabilities as reflected by the ΔΔOD transients. The points are the data and the lines are the fits. (c) The hole lifetimes showing the effect of decoupling the ligands from the quantum dot.

To further demonstrate the role of surface ligands, experiments were performed with ZnS capped CdSe quantum dots.[36] The ZnS shell will provide a tunneling barrier[73,74] which will attenuate the electronic coupling between the CdSe states and the ligands. Passivation of CdSe with two monolayers of ZnS clearly increases the time scale for hole relaxation from 248±10 to 335 fs, Fig. 7. The size and surface dependent transition rates demonstrate the importance of the surface ligands, which dominate the final stages of hole dynamics.

While these experiments spectroscopically probe the hole relaxation dynamics from the $2S_{3/2}$ initial state to the $1S_{3/2}$ final state, a subtlety in the level structure can be used to refine this picture. In more detail, there is an intermediate $1P_{3/2}$ state which is close to the $1S_{3/2}$ valence band edge state.[30–32] More rigorously, this experiment probes sequential kinetics for holes: $2S_{3/2} \rightarrow 1P_{3/2} \rightarrow 1S_{3/2}$. This simple kinetic scheme may be solved analytically or numerically to obtain the true state-to-state transition rates k_{32} and k_{21}. The subscripts refer to the ordering of the final and initial eigenstates, respectively. For simplicity, we assume that the numerator in the matrix element remains the same and the denominator changes to reflect the energy gaps. Thus, the measured time constant of 250 fs can be decomposed into sequential steps with time constants of 240 and 10 fs, respectively.

2. Hole energy loss rate through the valence band

The results here are specific to the final stage of hole relaxation. An understanding of the two primary pathways of hole relaxation can be extended to model *all* stages of hole relaxation. It is known that the density of hole states increases at higher energy.[10,25,26] Xu *et al.* previously estimated that the hole cooling rate slows as the hole approaches the band edge.[10] This cooling is due to the increasing level spacing near the band edge. While the current experiments show that there is no size induced bottleneck for holes, there should still be *slower* relaxation at the final stages of hole relaxation. Simply, both phonon and surface nonadiabatic relaxation pathways will be faster for the smaller level spacings expected at higher hole energy. Furthermore, higher energy hole state should have larger wave function overlap (due to tunneling and radial density) with the ligands, further increasing the magnitude of the ligand based channel. Thus, both mechanisms will necessarily produce more rapid hole relaxation at higher energy. However, these transitions are not *directly* detectable spectroscopically using the methods described here. These methods require specificity in the initial and final states. This condition is not possible to meet for the higher energy hole states. Yet, the principles deduced from the final stages of hole relaxation can be extended to predict all stages of hole relaxation.

The experiments here specifically probe hole dynamics for the lowest hole states. State-to-state transition rates can be determined by selectively exciting the initial excitonic state. The pump pulses can be tuned to be resonant with the hole in either the $1S_{3/2}$ or the $2S_{3/2}$ state. In both cases, the electron is in the $1S$ state, thereby allowing us to monitor only the dynamics of the hole. In contrast, excitation at higher photon energy would produce a mixture of hot electrons and hot holes for which extracting state-to-state dynamics would be difficult. However, the underlying picture of hole dynamics can be extended toward transitions between high energy hole states deep within the valence band.

The key point from the band edge results is that there are two primary pathways for hole relaxation in colloidal CdSe quantum dots. In the case of colloidal quantum dots, nonadiabatic transitions mediated by the surface ligands are the dominant relaxation channel. For each channel, the dependence on energy gap can be used to estimate the transition rates. A simple expression for the rate by phonon emission shows an exponential functional form, whereas a nonadiabatic channel has the rate going inversely with the square of the energy gap. Once the rates are known for one transition, the rate for each channel can be extended for any transition.

For example, the hole states have an energy difference of 50–100 meV near the band edge.[29–32] Deeper within the valence band, the hole level spacing decreases to 25–50 meV.[29–32] If the energy gap decreases by a factor of 2, the phonon channel would increase in rate by e^2 and the

nonadiabatic channel would increase by 2^2. At the band edge, the transition rate is 3.6 ps^{-1} for the nonadiabatic channel and 0.2 ps^{-1} for the phonon emission channel, for a total rate of 3.8 ps^{-1} (τ=260 fs). Simply by considering a smaller level spacing, the transition rates deeper in the valence band are expected to be ~14.4 and 1.6 ps^{-1}, respectively. Thus, the total transition rate deep in the valence band should be ~16.0 ps^{-1} (τ~60 fs). The hole energy loss rate increases from 0.3 eV/ps at the band edge to 0.6 eV/ps. Smaller hole level spacings will further increase the transition rate as well as the hole energy loss rate. These numbers are likely an underestimate of the transition rate for holes as *ab initio* works show that there is an increasing density of hole states deeper within the valence band.[25,26,75]

These extrapolated numbers can be compared to prior work. A quantum dynamics picture shows that the transition rate and energy loss rate will decrease as the hole approaches the band edge due to the increasing level spacing. On the other hand, there is no phonon bottleneck for holes in colloidal quantum dots due to the presence of additional femtosecond relaxation channels. This two channel quantum dynamics model can be extended to follow the hole cooling through the valence band using a sequential kinetics scheme, e.g.,

$$|h_4\rangle \xrightarrow{k_{43}} |h_3\rangle \xrightarrow{k_{32}} |h_2\rangle \xrightarrow{k_{21}} |h_1\rangle. \tag{10}$$

The state-to-state transition rate for each channel, e.g., k_{43}, is estimated from the measured transition rate at the band edge, k_{21}. The hole transition rates are adjusted based on the energy gaps[31,32] and computing the wave functions for the excited states. The rate of electron to hole energy transfer was taken from the experimentally determined transition rate for the electron. Solving the rate equations[76] produces the buildup time to the band edge as a function of the initial hole state,

$$\frac{dn_{2P_{3/2}}}{dt} = -k_{2P_{3/2}\to 1S_{1/2}} n_{2P_{3/2}} + k_{Auger} n_{1P_{3/2}}, \tag{11a}$$

$$\frac{dn_{1S_{1/2}}}{dt} = k_{2P_{3/2}\to 1S_{1/2}} n_{2P_{3/2}} - k_{1S_{1/2}\to 1P^{\ell}_{1/2}} n_{1S_{1/2}}, \tag{11b}$$

$$\frac{dn_{1P^{\ell}_{1/2}}}{dt} = k_{1S_{1/2}\to 1P^{\ell}_{1/2}} n_{1S_{1/2}} - k_{1P^{\ell}_{1/2}\to 2S_{3/2}} n_{1P^{\ell}_{1/2}}, \tag{11c}$$

$$\frac{dn_{2S_{3/2}}}{dt} = k_{1P^{\ell}_{1/2}\to 2S_{3/2}} n_{1P^{\ell}_{1/2}} - k_{2S_{3/2}\to 1P_{3/2}} n_{2S_{3/2}}, \tag{11d}$$

$$\frac{dn_{1P_{3/2}}}{dt} = k_{2S_{3/2}\to 1P_{3/2}} n_{2S_{3/2}} - k_{1P_{3/2}\to 1S_{3/2}} n_{1P_{3/2}}, \tag{11e}$$

$$\frac{dn_{1S_{3/2}}}{dt} = k_{1P_{3/2}\to 1S_{3/2}} n_{1P_{3/2}}. \tag{11f}$$

Figure 8 shows the hole dynamics through the valence band for a CdSe quantum dot of R=2.1 nm. Figure 8(a) shows the lifetime of each state based on the knowledge of the energy gaps.[31,32] In this case, the predicted lifetimes may be too large as the experimentally estimated hole level spacings used[31,32] are not necessarily more dense than at the band edge. On the other hand, *ab initio* works suggest greater density of hole states at higher excess energy.[25,26,77] Figure 8(b) shows the time scale ($1/e$) for arrival to the valence band edge as a function of the excess hole energy. The key feature is that the lowest energy hot hole ($1P_{3/2}$) actually has a longer time of arrival (T) to the cold hole state ($1S_{3/2}$). This result is specifically due to the electron-hole Auger energy transfer process which up pumps the hole. These results are in reasonable agreement with the time resolved terahertz experiments which measure the hole cooling time.[19] In general, the transition rate will scale approximately as $(\Delta E)^{-2}$ and the energy dissipation rate (dE/dt) will scale as $(\Delta E)^{-1}$. This functional form arises from the nonadiabatic contribution to the total rate. The hole energy loss rate predicted here is qualitatively consistent with the estimates of relaxation through the valence band from experiments by Xu *et al.*[10] and also consistent with the arrival time to the valence band edge based on terahertz experiments.[19]

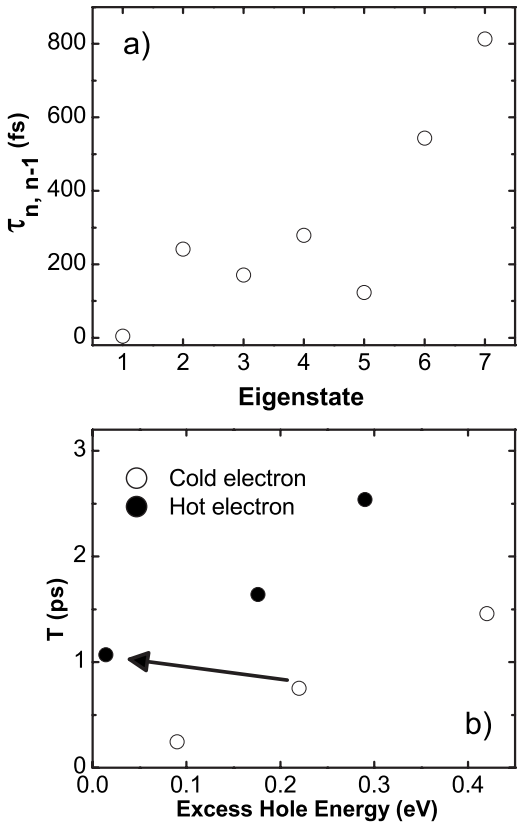

FIG. 8. Hole relaxation within the valence band for a CdSe quantum dot with R=2.1 nm. (a) The state-to-state lifetime (τ) as a function of the initial hole state. (b) The time to reach the valence band edge (T) as a function of excess hole energy. At higher photon energy, the electron is initially in a hot $1P$ state and the hole to a low energy $1P_{3/2}$ state. In this situation, the hole cooling is determined by electron-hole energy transfer via the Auger mechanism. The arrow denotes the increase in the hole cooling time due to the Auger process which transfers energy from the electron to the hole.

A final question is the vibrational mode specificity of the nonadiabatic relaxation process. There should be some

ligand degree of freedom which is resonant with the hole gaps and has appropriate symmetry to produce a nonvanishing numerator. Prior work has shown that ligand may be tuned to control electron dynamics in the absence of the Auger channel.[5] The key point is that there should be resonance between the electronic and the vibrational gaps as well as mode symmetry. These points will be addressed in future work.

B. Electron relaxation dynamics

1. Relaxation dynamics with a hole induced Auger channel

The size dependent electron relaxation process has been extensively discussed. However, none of the prior measurements reported on a state-to-state approach to electron relaxation dynamics. Prior transient absorption measurements used the band edge bleaching signal ($B1$) to monitor the electron populations. However, as the size of the quantum dot increases, the initial state for the electron will go from $1S$, $1P$, $2S$, etc., for a fixed pump wavelength of 400 nm (3.1 eV). For all but the smallest quantum dots, the measured transients would necessarily follow complex sequential kinetics, which are nonexponential. For this reason, fixed wavelength excitation could qualitatively demonstrate the size dependent electron relaxation rates but could not do so with the quantitative precision required to unambiguously establish the functional form of the size dependence.

A quantitative determination of the transition rate is essential for comparison to theory in order to critically assess the understanding of the Auger process in confined semiconductors. The decay rate for Coulomb mediated energy transfer from the electron to the hole follows[26]

$$k_{fi} = \frac{\Gamma}{\hbar}\sum_{n\alpha}\frac{|J(h_s,e_p;h_n,e_{s,\alpha})|^2}{(E_{e_p}-E_{e_s}+E_{h_n}-E_{h_s})^2+(\Gamma/2)^2}. \qquad (12)$$

The initial state corresponds to $|e_p,h_s\rangle$ and the final state is $|e_s,h_n\rangle$. The E's represent the energies and Γ represents the linewidth. The matrix element for the transition rate, M_{fi}, is given by the Coulomb integral J as follows:

$$J(j,k,l,m) = \sum_{\sigma\sigma'}\int\int \varphi_j^*(\vec{r},\sigma)\varphi_k^*(\vec{r}',\sigma') \times \frac{e^2}{\varepsilon(\vec{r},\vec{r}')|\vec{r}-\vec{r}'|}\varphi_l(\vec{r},\sigma)\varphi_m(\vec{r}',\sigma')d^3rd^3r'. \qquad (13)$$

The ϕ_i's are the single particle wave functions and ε represents the dielectric function. The initial theory[24] predicted that the rate is independent of size with a time constant of ~2 ps, whereas more recent *ab initio* work[26] produces a time scale of 100–500 fs, qualitatively consistent with the prior measurements that lack state-to-state specificity. One issue is that the computed transition rate is very sensitive to the material parameters.[24,26] For example, the rate will depend on the resonance between the electronic and hole levels as well as on the linewidths. As such, there can be large variations in the total transition rate computed as well as in the size dependence of the transition rate. The size dependence of the transition rate is of particular importance as it reflects the extent to which size dependent relaxation processes are rigorously understood.

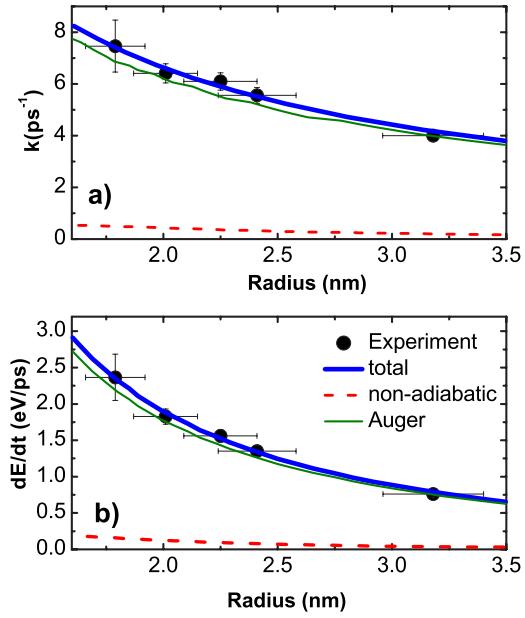

FIG. 9. (Color online) (a) The electron transition rate as a function of particle radius. (b) The electron energy loss rate (dE/dt) as a function of particle radius. The experiment selectively probes electron transitions from $1P \rightarrow 1S$. The electron transition rate from $1P \rightarrow 1S$ is linearly proportional to $1/R$. The total transition rate is the sum of all channels, where $k_{Auger} > k_{surface} \gg k_{phonon}$. When the hole is coupled to the electron, the Auger channel dominates the electron relaxation dynamics.

The 10 fs precision of these measurements warrants quantitative comparison to theory to verify our understanding of the precise mechanism for electron to hole energy transfer. Figure 9 shows the state-to-state transition rate for electrons as a function of particle radius. The precision of these experiments reveals that the functional form of the Auger-based transition rate is precisely $R^{-1.0\pm0.1}$. That the exponent is -1.0 ± 0.1 is essential to critically evaluate the details of the electronic structure which determines the Auger process in quantum dots.

Another point in evaluating the Auger process is to identify the correct states for the matrix elements. While the optically pumped initial excitonic state may be $1P_e$-$1P_{3/2}$, this is not necessarily the same as the initial state for the Auger process. The electron-hole energy transfer proceeds on the 100–300 fs time scale. However, the initial $1P_{3/2}$ hole will relax to the band edge in ~10 fs. Thus, the initial state for the Auger process is better represented by $1P_e$-$1S_{3/2}$. An *ab initio* approach[25,26,77] is required to properly address the consequences of this situation and to rigorously compare theory to experiment.

The experiment measures the total transition rate, where the total rate may be decomposed into the constituent channels. The surface ligands will necessarily mediate nonadiabatic transitions for the electrons with a size dependence for this channel that is similar to the observation for holes, Fig.

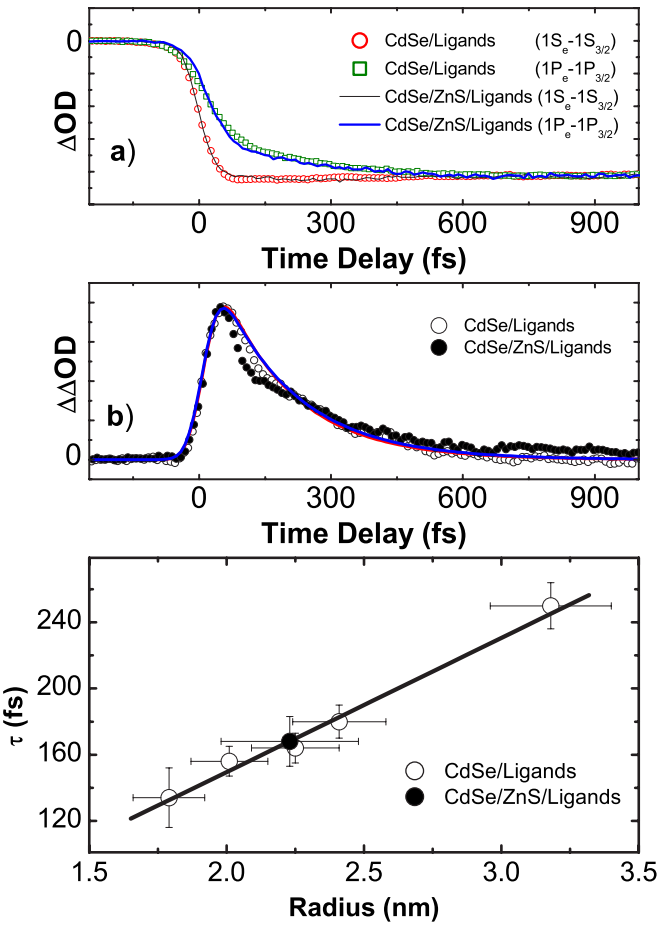

FIG. 10. (Color online) Effect of decoupling the surface ligands upon electron dynamics. (a) The pump-probe transients showing the effect of the ZnS tunneling barrier. The initial excitonic states are noted in parentheses. The transient labeled by the initial excitonic state $1P_e$-$1P_{3/2}$ also has contributions from $1S_e$-$2S_{1/2}$ as described in the text. (b) The electron survival probabilities as reflected by the ΔΔOD transients. The points are the data and the lines are the fits. (c) The electron lifetime showing the negligible effect of decoupling the ligands from the quantum dot. Ligand decoupling has a negligible effect on the electron dynamics since $k_{Auger} > k_{surface}$.

6. However, the energy gap for electrons is approximately three to four times larger; therefore, the transition rate will be approximately nine times smaller. If the holes have a nonadiabatic rate constant of $k_{fi} \sim 3-4$ ps^{-1}, then the electrons will have $k_{fi} \sim 0.2-0.4$ ps^{-1}. The experimental state-to-state transition rate is $\sim 4-8$ ps^{-1} over the measured range. For these sizes, electron relaxation from emission of phonons should be on the order of 50–500 ps,[2,21] giving a phonon based transition rate $k_{fi} \sim 0.01-0.1$ ps^{-1}. These ranges show that $k_{Auger} > k_{surface} > k_{phonon}$. Figure 9 shows the decomposition of the electron relaxation dynamics in terms of the two primary channels using the electron effective mass. The Auger channel is clearly the dominant relaxation pathway for electrons, provided that the hole is spatially coupled.

The proposition that the Auger channel dominates electron dynamics can be evaluated by decoupling of the surface ligands using the same ZnS tunneling barrier. Figure 10 shows that decoupling of the ligand has no effect (±10 fs) on the electron lifetime. This observation is reasonable considering the relative amplitudes of the Auger and the surface ligand induced channels. Thus, the *experimental* transition rate essentially probes *only* the Auger process under conditions in which the hole is coupled to the electron.

2. Quantum dynamical trajectories

As a final point, a complete trajectory may be mapped based on the knowledge of the electron and hole portions of the exciton relaxation pathways,

$$|1P_e - 1P_{3/2}\rangle \xrightarrow[NA]{k_1} |1P_e - 1S_{3/2}\rangle, \tag{14a}$$

$$|1P_e - 1S_{3/2}\rangle \xrightarrow[Auger]{k_2} |1S_e - 2P_{3/2}\rangle, \tag{14b}$$

$$|1S_e - 2P_{3/2}\rangle \xrightarrow[NA]{k_3} |1S_e - 1S_{3/2}\rangle. \tag{14c}$$

Optical excitation may be chosen to initially populate the $1P$-type exciton. In reality, this is not possible due to inhomogeneous and homogeneous broadenings causing the overlap of excitons consisting of hot and cold electrons. For the purposes of discussion, we consider only the case of the initial excitonic state being $1P$. The first step will be hole relaxation from $1P_{3/2}$ to $1S_{3/2}$, which proceeds on the 10 fs time scale primarily from surface ligand induced nonadiabatic transitions, k_1. The second step, k_2, corresponds to Auger-based electron to hole energy transfer, which proceeds on the 150–250 fs time scale. This process will up pump the hole to an excited state which is denoted as $2P_{3/2}$, maintaining conservation of energy in the Auger process. The specific up-pumped hole state may be different based on resonance conditions, but this case aims merely to illustrate one possible trajectory. The hot hole will eventually cool following sequential kinetics [Eq. (11)], k_3, to the band edge on the 1 ps time scale primarily from the nonadiabatic channel. The hot hole will initially undergo rapid state-to-state transitions deep within the valence band due to smaller level spacings. As the hole cools, the transition rate will slow, approximately following a $(\Delta E)^{-2}$ functional form. The hole cooling will necessarily be nonexponential since the hole undergoes sequential kinetics with at least four levels. With these ultrafast population dynamics, the effects of coherences[78] merit investigation since the lifetimes are approaching the dephasing time scales.[62,79]

3. Relaxation dynamics with a decoupled hole

Prior works have shown that surface ligands can control the rate of electron relaxation,[4,5,8] provided that the hole is decoupled from the electron. When the hole is spatially decoupled from the electron, the femtosecond Auger channel is removed, thereby yielding a picosecond surface dependent relaxation pathway for electrons in colloidal quantum dots. Upon scaling the nonadiabatic transition rate to the appropriate energy gap for electrons and using the electron effective

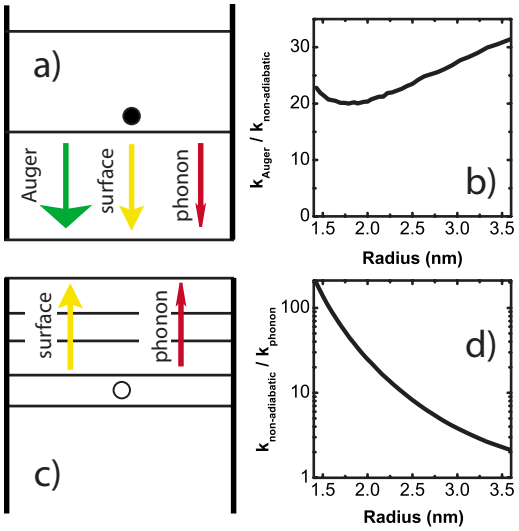

FIG. 11. (Color online) A multichannel picture of electron and hole relaxation dynamics in strongly confined semiconductor quantum dots. (a) The relaxation pathway for electrons involves three channels, where $k_{Auger} > k_{nonadiabatic} > k_{phonon}$. (b) The ratio $k_{Auger}/k_{nonadiabatic}$ for the two primary relaxation pathways for electrons. (c) The relaxation pathway for holes involves two channels, where $k_{nonadiabatic} > k_{phonon}$. (d) The ratio $k_{nonadiabatic}/k_{phonon}$ for the two primary relaxation pathways for holes.

mass, one expects a surface ligand induced nonadiabatic transition time of ~3–6 ps in CdSe colloidal quantum dots. This estimate matches well recent estimates of 3 ps using 100 fs laser pulses and 5–30 ps using 6 ps pulses. The relative contributions of the Auger and surface nonadiabatic channels are shown in Fig. 9.

In CdSe quantum dots, the hole induced Auger channel can be bypassed by spatially decoupling the hole to surface or trap states. In other materials such as PbSe, the hole spectrum has a more sparse level structure. As such, it was anticipated and experimentally verified that the electron relaxation times should be slower than in CdSe quantum dots due to a weaker Auger channel.[11,18] Assuming that there is no Auger channel for electrons in PbSe, the estimated electron lifetime based on the surface nonadiabatic channel is 1–3 ps, qualitatively consistent with the experimental results. A simple model with one adjustable scaling parameter can quantitatively reproduce the measured transition rate for holes in CdSe and can qualitatively reproduce the non-Auger-based transition rates for electrons in CdSe and PbSe.

C. Multichannel picture of exciton relaxation dynamics in quantum dots

Precision measurements of the state-to-state transition rate as a function of quantum dot size can be used to extract the mechanism(s) by which excited charge carriers relax. The key point is that there are multiple channels by which an electron or hole relaxes, Fig. 11. In the case of holes, it is clear that phonon emission cannot account for the final stages of relaxation in colloidal quantum dots. Thus, there are at least two channels for hole relaxation,

$$k(R)_{hole} = k(R)_{nonadiabatic} + k(R)_{phonon}. \quad (15)$$

In the case of electrons, recent pictures have focused on two channels for relaxation. The emission of LO phonons through the Fröhlich interactions was initially proposed.[1,2,22,23,27] Subsequent works have shown the presence of the femtosecond Auger channel in CdSe quantum dots.[1,2,24,26] In cases where the Auger channel was deactivated by spatial decoupling of the hole, a surface based relaxation channel was important for electrons. The surface channel for electrons was reported to be on the 1–30 ps time scale, depending on the choice of surface ligands.[4,5,8] The total relaxation rate for the electron will be the sum of these *three* relaxation channels,

$$k(R)_{electron} = k(R)_{Auger} + k(R)_{nonadiabatic} + k(R)_{phonon}. \quad (16)$$

The quantum dynamics underlying relaxation processes in quantum dots will necessarily be comprised of the *manifold* of pathways by which energy can be dissipated. Each pathway may furthermore have a distinct size dependence. These state-to-state measurements offer the quantitative precision necessary to evaluate the presence and relative amplitudes of the multiple relaxation channels. While state-to-state processes are standard in molecular dynamics, it is reasonable to extend these concepts to excitons in quantum dots.[20]

VI. CONCLUSIONS

The state-to-state transition rate for electrons and holes in strongly confined colloidal CdSe quantum dots is presented here. By using an exciton selective approach with 40 fs laser pulses, we achieve a combination of frequency resolution to pump specific initial excitonic states along with the requisite time resolution to measure all the relevant dynamical processes.

This exciton selective approach yields the size dependence of both electron and hole transitions near the band edge, holding the initial and final states for each size of quantum dot constant. The experiments on hole dynamics show an unexpected breaking of the "phonon bottleneck" for holes. The transition rate for holes is independent of particle size within the uncertainty of ±10 fs. This observation was rationalized in terms of a relaxation channel for holes: nonadiabatic transitions mediated by surface ligands. The transition rate for electrons was measured with quantitative precision of ±10 fs by maintaining the same states for each quantum dot. These experiments provide a critical test of theories for Auger processes in semiconductor quantum dots.

These experiments produce two broad conclusions on the manner in which an exciton relaxes in a quantum dot. Firstly, the relevant processes should be discussed in terms of state-to-state transitions rather than carrier cooling or energy loss rates. Since quantum dots have a resolvable eigenstate spectrum, a state-to-state language is more appropriate as in the case of quantum molecular dynamics. Secondly, there are multiple channels by which an electron or hole can relax in colloidal semiconductor quantum dots. Each of these channels has a size dependence that is distinct. The experimen-

tally observed size dependent transition rate corresponds to the sum of all transition rates for each channel. The key question is not what is the mechanism for electron or hole relaxation but rather what are the relative contributions of each channel to the total transition rate. Only by understanding the manifold of relaxation channels that are available in quantum dots can one rationally design the materials for specific applications.

ACKNOWLEDGMENTS

Financial support from the CFI, NSERC, FQRNT, and McGill University is acknowledged. We thank the McGill University Center for Self-Assembled Chemical Structures for use of their facilities. S.L.S. acknowledges support from James McPhee Foundation. E.A.D. acknowledges support from NSERC CGS-M.

*Author to whom correspondence should be addressed; Electronic address: pat.kambhampati@mcgill.ca

[1] V. I. Klimov, J. Phys. Chem. B **104**, 6112 (2000).
[2] A. J. Nozik, Annu. Rev. Phys. Chem. **52**, 193 (2001).
[3] U. Woggon, H. Giessen, F. Gindele, O. Wind, B. Fluegel, and N. Peyghambarian, Phys. Rev. B **54**, 17681 (1996).
[4] P. Guyot-Sionnest, M. Shim, C. Matranga, and M. Hines, Phys. Rev. B **60**, R2181 (1999).
[5] P. Guyot-Sionnest, B. Wehrenberg, and D. Yu, J. Chem. Phys. **123**, 074709 (2005).
[6] V. I. Klimov and D. W. McBranch, Phys. Rev. Lett. **80**, 4028 (1998).
[7] V. I. Klimov, D. W. McBranch, C. A. Leatherdale, and M. G. Bawendi, Phys. Rev. B **60**, 13740 (1999).
[8] V. I. Klimov, A. A. Mikhailovsky, D. W. McBranch, C. A. Leatherdale, and M. G. Bawendi, Phys. Rev. B **61**, R13349 (2000).
[9] V. I. Klimov, A. A. Mikhailovsky, D. W. McBranch, C. A. Leatherdale, and M. G. Bawendi, Science **287**, 1011 (2000).
[10] S. Xu, A. A. Mikhailovsky, J. A. Hollingsworth, and V. I. Klimov, Phys. Rev. B **65**, 045319 (2002).
[11] R. D. Schaller, J. M. Pietryga, S. V. Goupalov, M. A. Petruska, S. A. Ivanov, and V. I. Klimov, Phys. Rev. Lett. **95**, 196401 (2005).
[12] S. L. Sewall, R. R. Cooney, K. E. H. Anderson, E. A. Dias, and P. Kambhampati, Phys. Rev. B **74**, 235328 (2006).
[13] C. Burda and M. A. El-Sayed, Pure Appl. Chem. **72**, 165 (2000).
[14] C. Burda, S. Link, T. C. Green, and M. A. El-Sayed, J. Phys. Chem. B **103**, 10775 (1999).
[15] C. Burda, S. Link, M. Mohamed, and M. El-Sayed, J. Phys. Chem. B **105**, 12286 (2001).
[16] M. B. Mohamed, C. Burda, and M. A. El-Sayed, Nano Lett. **1**, 589 (2001).
[17] D. F. Underwood, T. Kippeny, and S. J. Rosenthal, J. Phys. Chem. B **105**, 436 (2001).
[18] J. M. Harbold, H. Du, T. D. Krauss, K.-S. Cho, C. B. Murray, and F. W. Wise, Phys. Rev. B **72**, 195312 (2005).
[19] E. Hendry, M. Koeberg, F. Wang, H. Zhang, C. de Mello Donega, D. Vanmaekelbergh, and M. Bonn, Phys. Rev. Lett. **96**, 057408 (2006).
[20] D. Scholes Gregory and G. Rumbles, Nat. Mater. **5**, 683 (2006).
[21] J. Urayama, T. B. Norris, J. Singh, and P. Bhattacharya, Phys. Rev. Lett. **86**, 4930 (2001).
[22] H. Benisty, C. M. Sotomayor-Torres, and C. Weisbuch, Phys. Rev. B **44**, 10945 (1991).
[23] U. Bockelmann and G. Bastard, Phys. Rev. B **42**, 8947 (1990).
[24] A. L. Efros, V. A. Kharchenko, and M. Rosen, Solid State Commun. **93**, 281 (1995).
[25] M. Califano, G. Bester, and A. Zunger, Nano Lett. **3**, 1197 (2003).
[26] L.-W. Wang, M. Califano, A. Zunger, and A. Franceschetti, Phys. Rev. Lett. **91**, 056404 (2003).
[27] S. S. Prabhu, A. S. Vengurlekar, S. K. Roy, and J. Shah, Phys. Rev. B **51**, 14233 (1995).
[28] T. Inoshita and H. Sakaki, Phys. Rev. B **46**, 7260 (1992).
[29] A. P. Alivisatos, J. Phys. Chem. **100**, 13226 (1996).
[30] A. L. Efros and M. Rosen, Annu. Rev. Mater. Sci. **30**, 475 (2000).
[31] D. J. Norris and M. G. Bawendi, Phys. Rev. B **53**, 16338 (1996).
[32] A. I. Ekimov, F. Hache, M. C. Schanne-Klein, D. Ricard, C. Flytzanis, I. A. Kudryavtsev, T. V. Yazeva, A. V. Rodina, and A. L. Efros, J. Opt. Soc. Am. B **10**, 100 (1993).
[33] V. I. Klimov, J. Phys. Chem. B **110**, 16827 (2006).
[34] A. J. Nozik, Inorg. Chem. **44**, 6893 (2005).
[35] A. Shabaev, A. L. Efros, and A. J. Nozik, Nano Lett. **6**, 2856 (2006).
[36] R. R. Cooney, S. L. Sewall, K. E. H. Anderson, E. A. Dias, and P. Kambhampati, Phys. Rev. Lett. **98**, 177403 (2007).
[37] J. J. Li, Y. A. Wang, W. Guo, J. C. Keay, T. D. Mishima, M. B. Johnson, and X. Peng, J. Am. Chem. Soc. **125**, 12567 (2003).
[38] W. W. Yu, L. Qu, W. Guo, and X. Peng, Chem. Mater. **15**, 2854 (2003).
[39] V. I. Klimov, C. J. Schwarz, D. W. McBranch, C. A. Leatherdale, and M. G. Bawendi, Phys. Rev. B **60**, R2177 (1999).
[40] P. Kambhampati, D.-H. Son, T. W. T. W. Kee, and P. F. Barbara, J. Phys. Chem. A **104**, 10637 (2000).
[41] Y. Z. Hu, S. W. Koch, M. Lindberg, N. Peyghambarian, E. L. Pollock, and F. F. Abraham, Phys. Rev. Lett. **64**, 1805 (1990).
[42] S. L. Sewall, R. R. Cooney, E. D. Dias, and P. Kambhampati (unpublished).
[43] D. H. Son, P. Kambhampati, T. W. Kee, and P. F. Barbara, J. Phys. Chem. A **105**, 8269 (2001).
[44] T. W. Kee, D. H. Son, P. Kambhampati, and P. F. Barbara, J. Phys. Chem. A **105**, 8434 (2001).
[45] I. B. Martini, E. R. Barthel, and B. J. Schwartz, Science **293**, 462 (2001).
[46] F. J. Webster, J. Schnitker, M. S. Friedrichs, R. A. Friesner, and P. J. Rossky, Phys. Rev. Lett. **66**, 3172 (1991).
[47] B. J. Schwartz and P. J. Rossky, J. Chem. Phys. **101**, 6917 (1994).
[48] C. Silva, P. K. Walhout, K. Yokoyama, and P. F. Barbara, Phys. Rev. Lett. **80**, 1086 (1998).
[49] K. Wynne and R. M. Hochstrasser, Adv. Chem. Phys. **107**, 263 (1999).

[50] J. C. Tully, J. Chem. Phys. **93**, 1061 (1990).
[51] J. C. Tully, Int. J. Quantum Chem. **S25**, 299 (1991).
[52] J. C. Tully, Annu. Rev. Phys. Chem. **51**, 153 (2000).
[53] M. Head-Gordon and J. C. Tully, J. Chem. Phys. **103**, 10137 (1995).
[54] K. Yokoyama, C. Silva, D. H. Son, P. K. Walhout, and P. F. Barbara, J. Phys. Chem. A **102**, 6957 (1998).
[55] L. J. Butler, Annu. Rev. Phys. Chem. **49**, 125 (1998).
[56] W. Domcke and G. Stock, Adv. Chem. Phys. **100**, 1 (1997).
[57] A. W. Jasper, S. Nangia, C. Zhu, and D. G. Truhlar, Acc. Chem. Res. **39**, 101 (2006).
[58] A. Stolow, Annu. Rev. Phys. Chem. **54**, 89 (2003).
[59] G. Hanna and R. Kapral, Acc. Chem. Res. **39**, 21 (2006).
[60] J. J. Shiang, S. H. Risbud, and A. P. Alivisatos, J. Chem. Phys. **98**, 8432 (1993).
[61] T. D. Krauss and F. W. Wise, Phys. Rev. B **55**, 9860 (1997).
[62] D. M. Mittleman, R. W. Schoenlein, J. J. Shiang, V. L. Colvin, A. P. Alivisatos, and C. V. Shank, Phys. Rev. B **49**, 14435 (1994).
[63] T. D. Krauss and F. W. Wise, Phys. Rev. Lett. **79**, 5102 (1997).
[64] J. J. Shiang, R. H. Wolters, and J. R. Heath, J. Chem. Phys. **106**, 8981 (1997).
[65] Δ is in units of dimensionless normal coordinates, whereas ΔQ has units of length.
[66] P. F. Barbara, T. J. Meyer, and M. A. Ratner, J. Phys. Chem. **100**, 13148 (1996).
[67] L. E. Brus, J. Chem. Phys. **79**, 5566 (1983).
[68] D. Dorfs, H. Henschel, J. Kolny, and A. Eychmueller, J. Phys. Chem. B **108**, 1578 (2004).
[69] S. A. Ivanov, J. Nanda, A. Piryatinski, M. Achermann, L. P. Balet, I. V. Bezel, P. O. Anikeeva, S. Tretiak, and V. I. Klimov, J. Phys. Chem. B **108**, 10625 (2004).
[70] S. Flugge, *Practical Quantum Mechanics* (Springer, Berlin, 1971).
[71] R. Englman, *Non-radiative Decay of Ions and Molecules in Solids* (North-Holland, Amsterdam, 1979).
[72] D. S. Boudreaux, F. Williams, and A. J. Nozik, J. Appl. Phys. **51**, 2158 (1980).
[73] D. Battaglia, B. Blackman, and X. Peng, J. Am. Chem. Soc. **127**, 10889 (2005).
[74] E. A. Dias, S. L. Sewall, and P. Kambhampati, J. Phys. Chem. C **111**, 708 (2007).
[75] A. Franceschetti, H. Fu, L. W. Wang, and A. Zunger, Phys. Rev. B **60**, 1819 (1999).
[76] The initial hole state used in the model was a fictitious state to avoid population feedback.
[77] M. Califano, A. Zunger, and A. Franceschetti, Nano Lett. **4**, 525 (2004).
[78] D. S. Chemla and J. Shah, Proc. Natl. Acad. Sci. U.S.A. **97**, 2437 (2000).
[79] M. R. Salvador, M. A. Hines, and G. D. Scholes, J. Chem. Phys. **118**, 9380 (2003).